

Polarization reversal *via* a transient relaxor state in nonergodic relaxors near freezing temperature

Chang-Hyo Hong^a, Hanzheng Guo^b, Xiaoli Tan^b, John E. Daniels^c, Wook Jo^{a,*}

^a School of Materials Science and Engineering, Ulsan National Institute of Science and Technology, Ulsan, 44919, Republic of Korea

^b Department of Materials Science and Engineering, Iowa State University, Ames, IA, 50011, USA

^c School of Materials Science and Engineering, University of New South Wales, New South Wales, 2052, Australia

ARTICLE INFO

Article history:

Received 18 April 2019

Received in revised form

7 June 2019

Accepted 24 June 2019

Available online 25 June 2019

Keywords:

Relaxor

Nanodomains

In situ

Neutron diffraction

Transmission electron microscopy

ABSTRACT

Among the unresolved issues in the study of relaxor ferroelectrics is the role of freezing temperature, across which the dynamics of polarization reversal in relaxor ferroelectrics changes. The presence of this freezing temperature is best manifested by the appearance of a double polarization hysteresis loop just above the freezing temperature. Given that the polarization pinching evolving into a double hysteresis starts well below the freezing temperature, there exists a transient temperature regime between the nonergodic and the ergodic relaxor states. To clarify the role of the freezing temperature on the pinching, the polarization reversal near the freezing temperature of relaxor $(\text{Pb}_{1-x}\text{La}_x)(\text{Zr}_{1-y}\text{Ti}_y)_{1-x/4}\text{O}_3$ (PLZT) was monitored using three *in situ* electric field methods: electrocaloric effect, neutron diffraction, and transmission electron microscopy. We demonstrate that the pinching results from a two-step process, 1) domain detexturization in the ferroelectric state and 2) miniaturization of domains. This observation explains the recently reported gap between the depolarization temperature T_d and the ferroelectric-to-relaxor transition temperature T_{F-R} in lead-free relaxors. We further show that T_d and T_{F-R} , which have long been considered identical in lead-based relaxors, are not the same. The current study suggests that the mismatch between T_d and T_{F-R} is an inherent feature in both lead-based and lead-free relaxor ferroelectrics.

© 2019 The Chinese Ceramic Society. Production and hosting by Elsevier B.V. This is an open access article under the CC BY-NC-ND license (<http://creativecommons.org/licenses/by-nc-nd/4.0/>).

1. Introduction

Relaxor ferroelectrics have been studied extensively due to their use in a versatile applications and also due to their intriguing physical phenomena that are yet to be clarified [1–3]. Among such intriguing phenomena is the existence of Vogel-Fulcher temperature (T_{VF}), commonly referred to as the freezing temperature (T_f) [4–7]. Below T_f , the longest relaxation time of polar nanoregions (PNRs) diverges [8]. A relaxor below T_f is called a nonergodic relaxor, while that above T_f is an ergodic relaxor [9]. Due to the dynamics of PNRs, a permanent long-range ferroelectric order can be induced in nonergodic relaxors with the application of an external electric field. Once this long-range ferroelectric order is induced, nonergodic relaxors are indistinguishable from normal ferroelectrics with respect to their functional properties such as

polarization and strain hysteresis. This electric-field-induced ferroelectric state in nonergodic relaxors is disturbed when they are heated up above the ferroelectric-to-relaxor transition temperature (T_{F-R}), where they transform into ergodic relaxors.

It is commonly known that this transition back to an ergodic relaxor state is accompanied by the appearance of an anomaly in both the real and the imaginary part of the dielectric permittivity [10]. Meanwhile, an electric field applied to a nonergodic relaxor induces a ferroelectric state and hence piezoelectricity. Therefore, from the piezoelectric point of view, a so-called depolarization temperature (T_d), commonly determined by thermally-stimulated depolarization current (TSDC) measurement [11,12], is of practical importance, as it marks the upper temperature limit for piezoelectric applications. On the other hand, the presence of T_d is also well-reflected in the thermal evolution of polarization hysteresis loops. As the temperature is increased to near T_f , the polarization hysteresis loop of nonergodic relaxors starts to be pinched, resulting in a double-loop polarization hysteresis. The appearance of double-loop polarization hysteresis is not unique in relaxor systems since the double-loop polarization hysteresis merely

* Corresponding author.

E-mail address: wookjo@unist.ac.kr (W. Jo).

Peer review under responsibility of The Chinese Ceramic Society.

requires a macroscopic paraelectric state at zero field [13]. It is noted that the pinched hysteresis loop near T_f is different from the double hysteresis loop of defect-induced relaxors [14,15], which usually de-pinches after successive electrical cycling [16–18]. The pinched hysteresis of relaxors implies that near T_f , the polarization reversal takes place in two steps, i.e., the polarization reversal involves a transient macroscopic relaxor state [19]. In principle, the depoling electric field E_d , where the induced polarization starts to vanish during unloading electric field (See, for example, Fig. 1 for the meaning of notations used in the current work) reaches 0 kV/mm at T_d .

So far, in canonical relaxors such as $\text{Pb}(\text{Mg}_{1/3}\text{Nb}_{2/3})\text{O}_3$ (PMN) [20–22] and $(\text{Pb}_{1-x}\text{La}_x)(\text{Zr}_{1-y}\text{Ti}_y)_{1-x/4}\text{O}_3$ (PLZT) [13,23,24], T_f , T_d , and T_{F-R} have been considered to be the same. However, a number of recent experimental works on lead-free compositions suggest that T_{F-R} does not have to be identical with T_d [19,25,26]. It implies that the depolarization and the transition to the ergodic relaxor state of electrically-induced ferroelectric state are separate processes. In fact, it was demonstrated in $0.94(\text{Bi}_{1/2}\text{Na}_{1/2})\text{TiO}_3$ -0.06BaTiO₃ (94BNT-6BT) that the process taking place across T_d and then T_{F-R} is a detexturization of electrically aligned ferroelectric domains, followed by the miniaturization of the detexturized ferroelectric domains with a long-range order [13,19,25]. This means that the thermal energy required for depolarizing the electrically textured state is smaller than that for disrupting electrically-induced long-range ferroelectric order. As aforementioned, these stepwise processes are absent in normal ferroelectrics [27,28]. Given this, the polarization reversal near T_d should, in fact, occur in three steps: 1) poled state decays into randomly oriented domains, 2) detexturized ferroelectric state breaks down to macroscopic relaxor state, 3) textured ferroelectric state aligned in the opposite direction is manifested [29]. Here, we demonstrate that the polarization reversal near T_d , indeed, takes place in three steps, using calorimetry, neutron diffraction, and transmission electron microscopy.

2. Experimental

Hot-pressed commercially available PLZT8/65/35 (Boston Applied Technologies, MA, USA) was used for this study. For

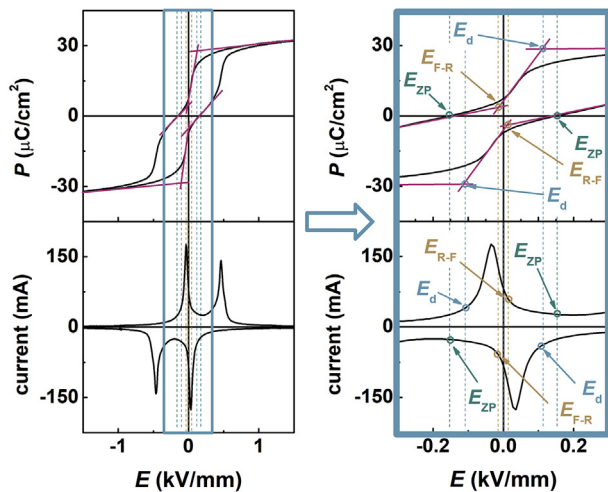


Fig. 1. Intersections of linear extrapolation lines of saturated polarization and pinched polarization curves were used to specify the stepwise polarization reversal process via a ferroelectric-to-relaxor state. Notation E_d , E_{F-R} , and E_{R-F} denote depoling electric field, transition electric field from the ferroelectric-to-relaxor state, and relaxor-to-ferroelectric state, respectively. The zero polarization electric field E_{ZP} is used instead of the coercive field E_C where depolarization takes place in typical ferroelectrics.

comparison purpose, a commercial soft PZT (PIC 151, PI Ceramic, Lederhose, Germany) and self-made $0.94(\text{Bi}_{1/2}\text{Na}_{1/2})\text{TiO}_3$ -0.06BaTiO₃ (BNT-6BT) [30] were also utilized.

Electrocaloric effects were quantified by a direct measurement method using a homemade *in situ* calorimeter which consists of a vacuum bottle, silicone oil, and a temperature sensor (Pt 100, Heraeus Sensor Technology GmbH, Germany). The temperature sensor was directly attached to the sample surface. The triangular bi-polar electric field was applied at 0.1 Hz by a power supply (20/20C, Trek, Inc. USA). Polarization hysteresis and switching current loops were obtained with a piezoelectric evaluation system (aixPES, AixACCT, Germany).

Neutron diffraction experiments were carried out using the Wombat powder diffractometer at the Australian Nuclear Science and Technology Organisations OPAL research reactor. A neutron wavelength of 2.41 Å was used. A detailed description of the experimental geometry is available in Ref. [31]. As there may be some time-dependence to the switching behavior observed in PLZT, we performed time-resolved investigations using a stroboscopic technique. We applied a triangular waveform at 0.1 Hz where the detected neutrons are sampled into time bins associated with the field at an instantaneous point in time. The data collection combines the sum of many cycles of the waveform. The maximum applied field was 700 V/mm for the sample at 23 °C (room temperature) and 500 V/mm for the sample at 40 °C (above T_{F-R}).

For *in situ* electric field transmission electron microscopy (TEM), disk specimens were prepared through standard procedures including grinding, cutting, dimpling, and ion milling. The dimpled disks were annealed at 200 °C for 2 h to minimize the stress-induced effects prior to Ar-ion milling to electron transparency. *In situ* TEM experiments were carried out on a specimen that was crack-free at the edge of the central perforation on a Phillips CM30 microscope operated at 200 kV. Experimental details can be found in Refs. [32–34].

3. Results and discussion

3.1. Electrocaloric effect

Polarization hysteresis, switching current, and electrocaloric effect of a commercial PZT (PIC 151, PI Ceramic, Lederhose, Germany) and PLZT ceramics during electrical cycling at room temperature are compared in Fig. 2. For both PIC 151 and PLZT, the initial increase in the polarization value is due to the formation of a textured long-range order induced by the application of the external electric field, accompanied by electrocaloric heating. During a reverse cycle, PIC 151 reveals typical ferroelectric polarization switching with a single switching current, while two discrete peaks are noted in the switching current for PLZT. It is obvious from the temperature change that the first peak, making the polarization state vanished, is related to the transition of the electric-field-induced ferroelectric state back to the original relaxor state [19,35], and the second one stems from the establishment of a textured long-range order along the reverse direction. It is noted that the adiabatic cooling comes from the electromechanical work, devoting to the disruption of the poled state of the electric-field-induced ferroelectric phase [36–38].

3.2. Neutron diffraction

The structure of as-sintered PLZT is observed to be near cubic using neutron diffraction without any discerned peak splitting nor superlattice reflections (Fig. 3), which is typical for relaxor ferroelectrics [39–43]. As will be shown later, the TEM study confirmed that at a local scale, the initial state of the material is a

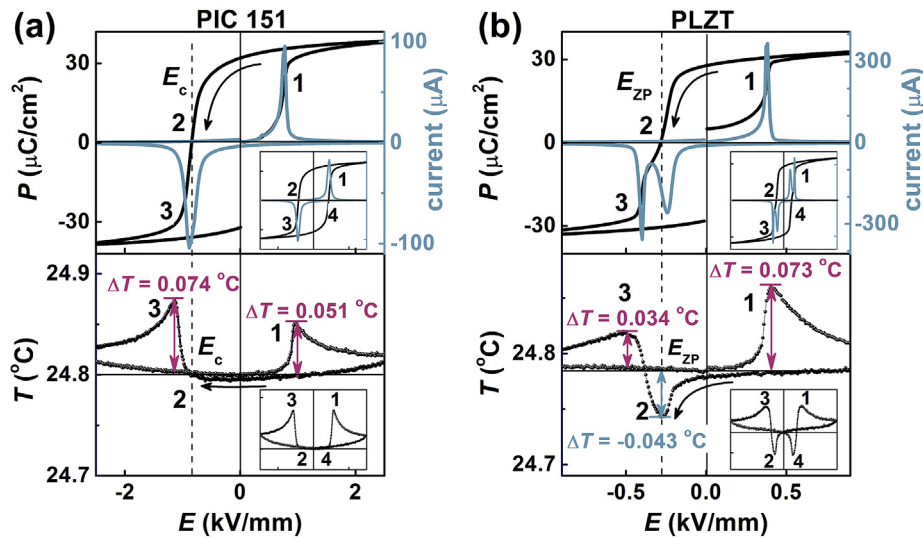


Fig. 2. Polarization hysteresis and switching current compared with the electrocaloric effect of (a) PIC151 and (b) PLZT in an initial unpoled state. Inset figures show the second cycle.

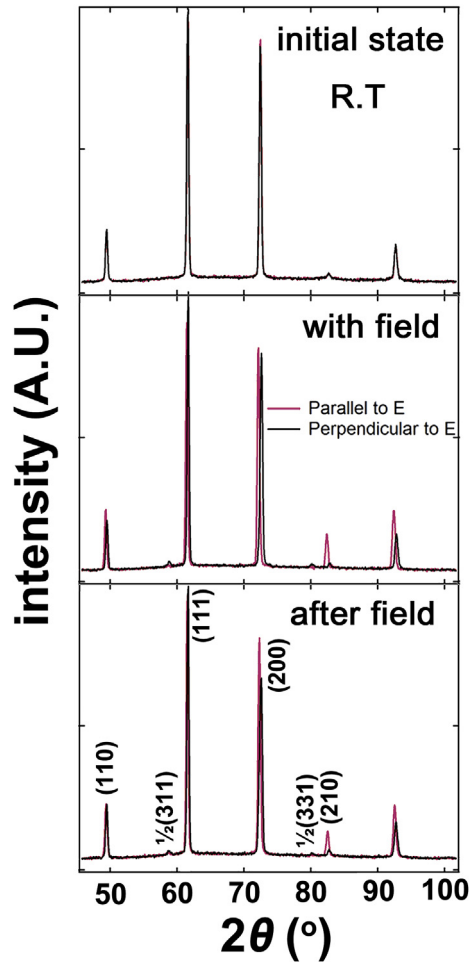


Fig. 3. Change in structure by electrical poling from the unpoled state at 23 °C and maximum field of 2 kV/mm.

rhombohedral $R3m$. It is reasonable to assume that the correlation length of the initially existing oxygen octahedral tilts manifested by superlattice reflections is below the detection limit of the currently

utilized neutron diffraction technique; albeit, detectable through a selected area electron diffraction (SAED) as will be presented later.

The application of electric fields at room temperature leads to the development of a significant lattice strain and the appearance of $\frac{1}{2}(311)$ and $\frac{1}{2}(3\bar{1}1)$ superlattice reflections when the scattering vector is aligned along the electric field direction. The appearance of superlattice reflections is most likely associated with an anti-phase oxygen octahedral tilting ($a^-a^-a^-$). As presented in Fig. 4, the observed change in the diffraction pattern, e.g., an increase in the intensity of (210) with the appearance of $\frac{1}{2}(000)$ type superlattice reflections is best-explained, when the initial and the electric-field-induced phase are a macroscopically rhombohedral $R3m$ and $R3c$, respectively. Note that this does not necessarily mean that the entire material underwent this phase transformation. All grains within the polycrystal are aligned at different orientations to the electric field, and thus can be in different states under the field. The induced superlattice reflections along the field direction do not vanish after the removal of electric field, demonstrating that the electric-field-induced structural changes in this PLZT sample are irreversible at room temperature.

The (210) intensity as a function of applied electric field at 23 °C (room temperature) and 40 °C (above T_{F-R}) are presented in Fig. 5 (a) and (b) respectively. The (210) intensity at 23 °C features the typical ferroelectric strain curve. At 40 °C, the shape changes to a sprout-shaped strain curve with little remnant strain in the lattice, which is commonly observed in ergodic relaxors. It is noticed that there exists a strong correlation between the intensity of $\frac{1}{2}(311)$ and (210) reflections and the strain behavior. The intensity of both reflections starts to decrease near E_d and becomes the minimum near E_{F-R} .

3.3. Transmission electron microscopy

Using an *in situ* TEM technique, the electric-field-induced phase transitions are directly imaged and displayed in Fig. 6 on a representative grain along its $\langle 112 \rangle$ -zone axis. It is noted that the central perforation in the TEM specimen distorts the electric field [33,34]. As depicted in Fig. 6 (a), at virgin state, it consists of typical polar nanodomains. The corresponding SAED pattern [Fig. 6 (b)] reveals the presence of very weak $\frac{1}{2}\{000\}$ superlattice diffraction spots (o stands for odd Miller indices), which supports our designation of

Table 1
Fullprof simulation parameter for R3m and R3c.

		x	y	z	Occ.		
R3m	Pb	0	0	0	0.5		
	La	0	0	0	0.5		
	Zr	0	0	0.5	0.5		
	Ti	0	0	0.5	0.5		
R3c	O	0.16667	0.33333	0.33333	2.4		
	Pb	0	0	0.25	0.5		
	La	0	0	0.25	0.5		
	Zr	0	0	0	0.5		
	Ti	0	0	0	0.5		
	O	0.12	0.78667	0.08333	2.4		
	λ (Å)	a (Å)	b (Å)	c (Å)	α (°)	β (°)	γ (°)
R3m	2.41	5.77473	5.77473	7.08165	90	90	120
R3c	2.41	5.77473	5.77473	14.15724	90	90	120

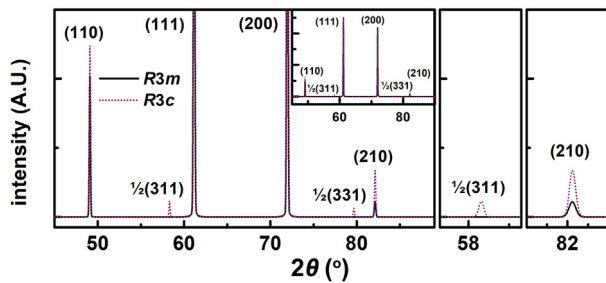


Fig. 4. Comparison of the neutron diffraction pattern simulation between R3m and R3c (Parameters used in the simulation are presented in Table 1).

R3c instead of R3m to as-sintered PLZT. Close-up examination of the portion of the SAED pattern for the fundamental diffraction ($\bar{2}22$) and the superlattice diffraction spot $\frac{1}{2}(3\bar{3}3)$ is displayed in Fig. 6 (c). The ($\bar{2}22$) spot features a circular shape, while the $\frac{1}{2}(3\bar{3}3)$ superlattice spot is weak and diffuse.

Electric fields with increasing magnitude were applied along the direction indicated by the bright arrow in Fig. 6 (d). At a field corresponding to point 'd' in Fig. 6 (m), the nanodomains begin to coalesce and cluster in the upper right region of the grain, and transform into long and thin domains on the left as well as lower

part of the grain [Fig. 6 (d)]. Compared with the crystallographic orientations revealed in the SAED in Fig. 6 (b), these domains are likely to have their walls on the ($\bar{1}10$) plane. With further increased electric field up to the field corresponding to point 'e' in Fig. 6 (m) [Fig. 6 (e)], the long and thin domains become broader and wedge-shaped, occupying most part of the grain. The domain walls remain roughly along the same ($\bar{1}10$) plane. Fig. 6 (a), 6 (d), and 6 (e) reveal the electric-field-induced relaxor-to-ferroelectric phase transition process in PLZT8/65/35 at room temperature. The coalescence of nanodomains and the formation of ($\bar{1}10$) wedge-shaped ferroelectric domains during the phase transition is consistent with our previous study on a $\text{Pb}(\text{Mg}_{1/3}\text{Nb}_{2/3})\text{O}_3$ -based relaxor composition [44,45]. Formation of large wedge-shaped ferroelectric domains is accompanied by a significant intensification of the $\frac{1}{2}\{000\}$ superlattice reflection spots [Fig. 6 (f)], which is highlighted in Fig. 6 (g) where the same ($\bar{2}22$) and $\frac{1}{2}(3\bar{3}3)$ spots are provided again. Note that the ($\bar{2}22$) fundamental diffraction spot is evidently distorted along the direction that is normal to the ($\bar{1}10$) domain walls, appearing as two split spots. The bright-field image of the grain after the applied field was removed for 1 h is presented in Fig. 6 (h). The preservation of the large ferroelectric domains confirms that the induced ferroelectric phase is sustained in the absence of an applied electric field and the relaxor-to-ferroelectric phase transition in PLZT8/65/35 is irreversible at room temperature.

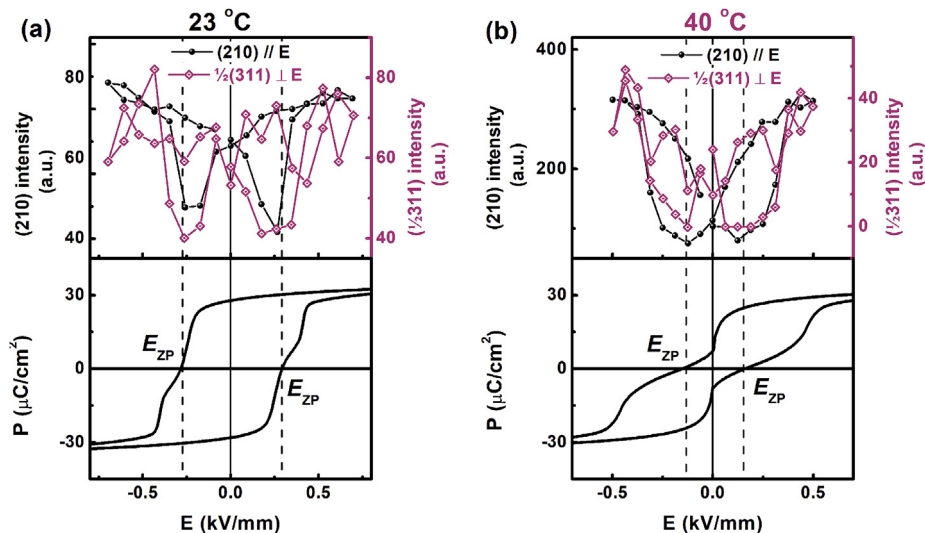


Fig. 5. The $\frac{1}{2}(311)$ and (210) peak intensity, and polarization hysteresis of PLZT at (b) 23 °C and (c) 40 °C as a function of applied electric field.

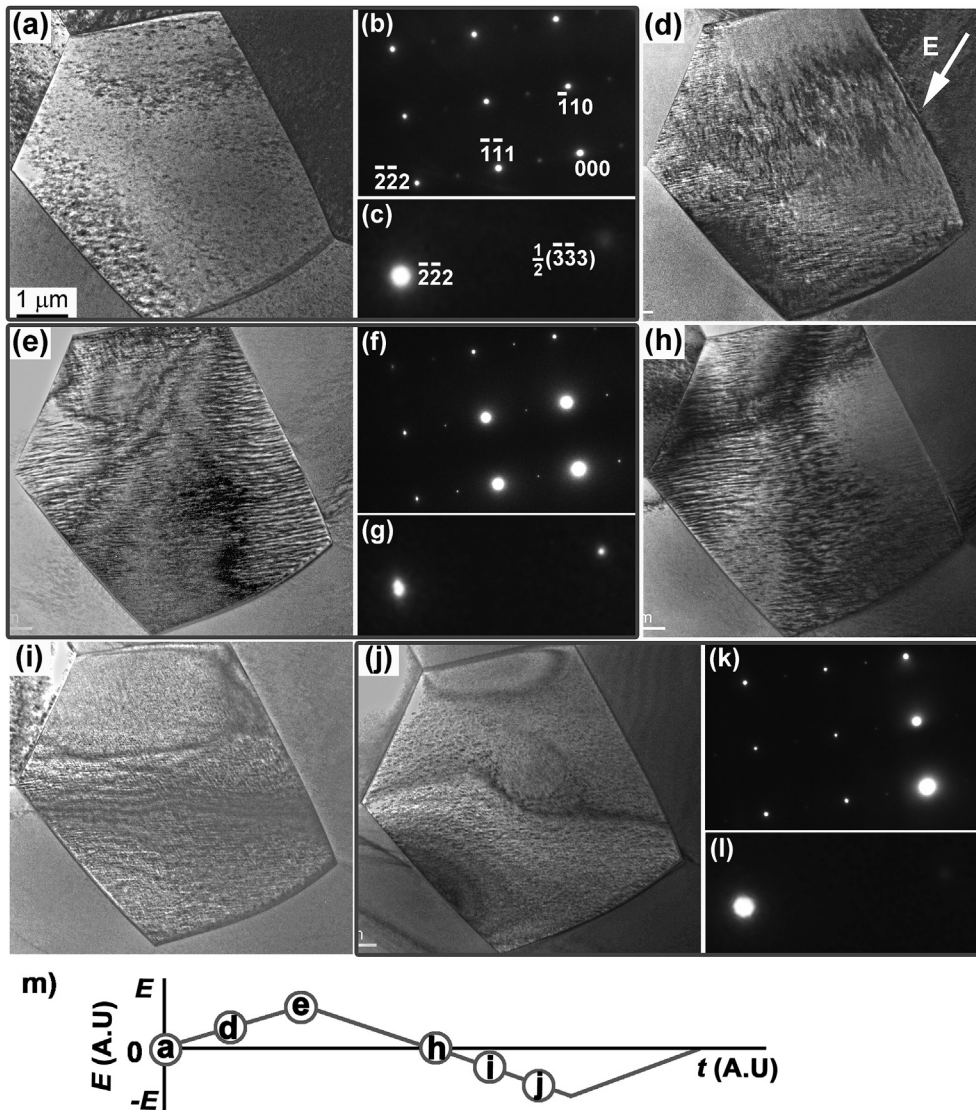


Fig. 6. *In situ* TEM direct observation on the electric-field-induced relaxor-to-ferroelectric and the ferroelectric-to-relaxor phase transitions from a grain along the $\langle 112 \rangle$ -zone axis in PLZT8/65/35. (a) The polar nanodomains at virgin state, (b) the SAED pattern at virgin state, (c) the magnified view of the (222) fundamental spot and the $\frac{1}{4}(333)$ superlattice spot at virgin state. (d) Under the field corresponds to point 'd' in (m); (e), (f), and (g) under the field 'e'; (h) the applied field returns to 0 kV/mm; (i) under the field 'i' (close to E_{F-R}); (j), (k), and (l) under the field 'j' (close to E_{ZP}). (m) a schematic paragraph of the applied fields. The SAED in (f) and (k) are the same portion of the diffraction pattern shown in (b), while (g) and (l) show the same spots as in (c).

The *in situ* TEM experiment directly reveals that the polarization reversal takes place through a ferroelectric-to-relaxor phase transition. As displayed in Fig. 6 (i), when the field in the reverse polarity close to E_{F-R} is applied, the large ferroelectric domains are disrupted into thin and short domains clustering in the same direction. In addition, nanodomains clustering along a different direction are also formed. At a field in the reverse direction corresponding to E_{ZP} , almost the entire grain is occupied with relaxor nanodomains [Fig. 6 (j)]. At the same time, the SAED pattern similar to that formed at virgin state is seen with circularly shaped fundamental spots and extremely weak superlattice spots [Fig. 6 (k) and (l)]. Further increase in the field magnitude in the reverse direction was observed to transform these nanodomains into large ferroelectric domains again, completing the polarization reversal process.

3.4. Field dependence of T_d and T_{F-R}

The correlation between T_d - T_{F-R} and E_d - E_{F-R} for (a) PLZT and (b) BNT-6BT is outlined in Fig. 7. It is reasonable to assume that T_d and

T_{F-R} should be defined at the point where E_d and E_{F-R} (Fig. 1) become zero, respectively. The former and the latter coincide with the temperature, where the detexturization of ferroelectric domains (T_d/E_d) and the miniaturization of detexturized ferroelectric domains (T_{F-R}/E_{F-R}) take place, respectively. In this sense, we notice that T_d is located at the temperature near the onset point of thermally-stimulated depolarization instead of the inflection point, i.e., the peak of TSDC. The dielectric anomaly, which has commonly been taken as T_{F-R} , takes place slightly below the actual T_{F-R} .

4. Conclusions

A stepwise polarization reversal process via a ferroelectric to a relaxor state was observed in a nonergodic relaxor PLZT using *in situ* monitoring methods, namely, electrocalorimetry, neutron diffraction, and TEM measurements. A room-temperature electrocaloric analysis on the ceramic revealed that in addition to commonly expected electrocaloric heating peaks correlated with the development or reversal of domain texture, there existed an

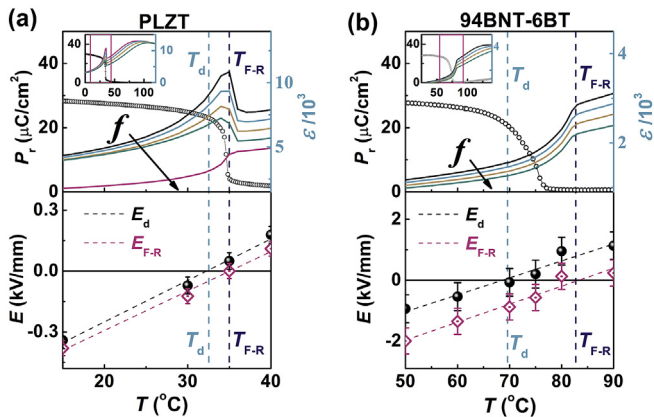


Fig. 7. Changes in the remanent polarization and the dielectric permittivity of electric-field-induced ferroelectric phase in (a) PLZT and (b) 94BNT-6BT with increasing temperature in comparison with T_d and T_{F-R} extracted from temperature-dependent polarization hysteresis loops (bottom). Error bars were determined by the standard error of intercept of the linear polynomial fit.

extra cooling peak in-between two heating ones. *In situ* neutron diffraction study revealed that the extra cooling peak correlated with the vanishing of the electric-field-induced $\frac{1}{2}(000)$ superlattice reflections, which implies that there exists an intermediate process breaking down the electric-field-induced long-range order during polarization reversal. *In situ* TEM study further demonstrated that the initial unpoled state consisted of polar nanodomains, which coalesced into well-developed ferroelectric domains by the application of electric field; under reverse fields, the electric-field-induced ferroelectric domains were disrupted into polar nanodomains similar to those in the initial state. The current study suggests that T_d and T_{F-R} do not have to be identical. A comparative study of both temperature-dependent and electrically-induced phase transitions verified that the deviation between T_d and T_{F-R} is quantified by the gap between the depoling electric field (E_d) and a phase transition electric field (E_{F-R}).

Acknowledgements

WJ is thankful for the financial support by the Basic Science Research Program through the National Research Foundation of Korea (NRF) funded by the Ministry of Education (NRF-2018R1D1A1B07051176). XT acknowledges the financial support by the National Science Foundation (NSF) through Grant DMR-1700014, and JD thanks the financial support from the ARC Discovery Project Scheme. We all acknowledge the support of the Australian Centre for Neutron Scattering, Australian Nuclear Science and Technology Organisation in providing the neutron research facilities used in this work.

References

- [1] Haertling GH. Ferroelectric ceramics: history and technology. *J Am Ceram Soc* 1999;82(4):797–818.
- [2] Hlinka J. Do we need the ether of polar nanoregions? *J Adv Dielectr* 2012;02(02):1241006.
- [3] Kleemann W. Random fields in relaxor ferroelectrics — a jubilee review. *J Adv Dielectr* 2012;02(02):1241001.
- [4] Viehland D, Li JF, Jang SJ, Cross LE, Wuttig M. Dipolar-glass model for lead magnesium niobate. *Phys Rev B* 1991;43(10):8316–20.
- [5] Viehland D, Jang SJ, Cross LE, Wuttig M. Freezing of the polarization fluctuations in lead magnesium niobate relaxors. *J Appl Phys* 1990;68(6):2916–21.
- [6] Ke S, Fan H, Huang H. Revisit of the Vogel–Fulcher freezing in lead magnesium niobate relaxors. *Appl Phys Lett* 2010;97(13):132905.
- [7] Pirc R, Kutnjak Z. Freezing in relaxor ferroelectrics and dipolar glasses. *Phase Transitions* 2015;88(3):222–33.
- [8] Tagantsev AK. Vogel–Fulcher relationship for the dielectric permittivity of relaxor ferroelectrics. *Phys Rev Lett* 1994;72(7):1100–3.

- [9] Bobnar V, Kutnjak Z, Pirc R, Levstik A. Electric-field-temperature phase diagram of the relaxor ferroelectric lanthanum-modified lead zirconate titanate. *Phys Rev B: Condens Matter* 1999;60(9):6420–7.
- [10] Bobnar V, Kutnjak Z, Pirc R, Levstik A. Relaxor freezing and electric-field-induced ferroelectric transition in a lanthanum lead zirconate titanate ceramics. *EPL (Europhys Lett)* 1999;48(3):326.
- [11] Anton E-M, Jo W, Damjanovic D, Rödel J. Determination of depolarization temperature of $(\text{Bi}_{1/2}\text{Na}_{1/2})\text{TiO}_3$ -based lead-free piezoceramics. *J Appl Phys* 2011;110(9):094108.
- [12] Zhao J, Zhang N, Ren W, Niu G, Walker D, Thomas Pamela A, Wang L, Ye Z-G. Polar domain structural evolution under electric field and temperature in the $(\text{Bi}_{0.5}\text{Na}_{0.5})\text{TiO}_3$ -0.06BaTiO₃ piezoceramics. *J Am Ceram Soc* 2019;102(1):437–47.
- [13] Jo W, Dittmer R, Acosta M, Zang J, Groh C, Sapper E, Wang K, Rödel J. Giant electric-field-induced strains in lead-free ceramics for actuator applications — status and perspective. *J Electroceram* 2012;29(1):71–93.
- [14] Ke SM, Huang HT, Fan HQ, Lee HK, Zhou LM, Mai Y-W. Antiferroelectric-like properties and enhanced polarization of Cu-doped $\text{K}_{0.5}\text{Na}_{0.5}\text{NbO}_3$ piezoelectric ceramics. *Appl Phys Lett* 2012;101(8):082901.
- [15] Shi J, Fan H, Liu X, Li Q. Giant strain response and structure evolution in $(\text{Bi}_{0.5}\text{Na}_{0.5})_{0.945-x}(\text{Bi}_{0.2}\text{Sr}_{0.7}\text{□}_{0.1})_{0.055}\text{Ba}_{0.055}\text{TiO}_3$ ceramics. *J Eur Ceram Soc* 2014;34(15):3675–83.
- [16] Carl K, Hardtl KH. Electrical after-effects in $\text{Pb}(\text{Ti}, \text{Zr})\text{O}_3$ ceramics. *Ferroelectrics* 1977;17(1):473–86.
- [17] Granzow T, Suvaci E, Kungl H, Hoffmann MJ. Deaging of heat-treated iron-doped lead zirconate titanate ceramics. *Appl Phys Lett* 2006;89(26):262908.
- [18] Hong C-H, Kim H-P, Choi B-Y, Han H-S, Son JS, Ahn CW, Jo W. Lead-free piezoceramics — where to move on? *J Materiomics* 2016;2(1):1–24.
- [19] Jo W, Daniels J, Damjanovic D, Kleemann W, Rödel J. Two-stage processes of electrically induced-ferroelectric to relaxor transition in $0.94(\text{Bi}_{1/2}\text{Na}_{1/2})\text{TiO}_3$ -0.06BaTiO₃. *Appl Phys Lett* 2013;102(19):192903.
- [20] Calvarin G, Hussen E, Ye ZG. X-ray study of the electric field-induced phase transition in single crystal $\text{Pb}(\text{Mg}_{1/3}\text{Nb}_{2/3})\text{O}_3$. *Ferroelectrics* 1995;165(1):349–58.
- [21] Ye Z-G, Schmid H. Optical, dielectric and polarization studies of the electric field-induced phase transition in $\text{Pb}(\text{Mg}_{1/3}\text{Nb}_{2/3})\text{O}_3$ [PMN]. *Ferroelectrics* 1993;145(1):83–108.
- [22] Cheng ZY, Katiyar RS, Yao X, Guo A. Dielectric behavior of lead magnesium niobate relaxors. *Phys Rev B* 1997;55(13):8165–74.
- [23] Farhi R, Marssi ME, Dellis JL, Picot JC, Morell A. On the nature of the glassy state in $9/65/35$ PLZT ceramics. *Ferroelectrics* 1996;176(1):99–106.
- [24] Schaab S, Granzow T. Temperature dependent switching mechanism of $(\text{Pb}_{0.92}\text{La}_{0.08})(\text{Zr}_{0.65}\text{Ti}_{0.35})\text{O}_3$ investigated by small and large signal measurements. *Appl Phys Lett* 2010;97(13):132902.
- [25] Sapper E, Schaab S, Jo W, Granzow T, Rödel J. Influence of electric fields on the depolarization temperature of Mn-doped $(1-x)\text{Bi}_{1/2}\text{Na}_{1/2}\text{TiO}_3$ - $x\text{BaTiO}_3$. *J Appl Phys* 2012;111(1):014105.
- [26] Bai W, Chen D, Zheng P, Shen B, Zhai J, Ji Z. Composition- and temperature-driven phase transition characteristics and associated electromechanical properties in $\text{Bi}_{0.5}\text{Na}_{0.5}\text{TiO}_3$ -based lead-free ceramics. *Dalton Trans* 2016;45(20):8573–86.
- [27] Daniels JE, Cozzan C, Ukritnukun S, Tutuncu G, Andrieux J, Glaum J, Dosch C, Jo W, Jones JL. Two-step polarization reversal in biased ferroelectrics. *J Appl Phys* 2014;115(22):224104.
- [28] Genenko YA, Khachatryan R, Schultheiß J, Ossipov A, Daniels JE, Koruza J. Stochastic multistep polarization switching in ferroelectrics. *Phys Rev B* 2018;97(14):144101.
- [29] Glaum J, Simons H, Hudspeth J, Acosta M, Daniels JE. Temperature dependent polarization reversal mechanism in $0.94(\text{Bi}_{1/2}\text{Na}_{1/2})\text{TiO}_3$ -0.06Ba $(\text{Zr}_{0.02}\text{Ti}_{0.98})\text{O}_3$ relaxor ceramics. *Appl Phys Lett* 2015;107(23):232906.
- [30] Hong C-H, Fan Z, Tan X, Kang W-S, Ahn CW, Shin Y, Jo W. Role of sodium deficiency on the relaxor properties of $\text{Bi}_{1/2}\text{Na}_{1/2}\text{TiO}_3$ -BaTiO₃. *J Eur Ceram Soc* 2018;38(16):5375–81.
- [31] Simons H, Daniels JE, Studer AJ, Jones JL, Hoffman M. Measurement and analysis of field-induced crystallographic texture using curved position-sensitive diffraction detectors. *J Electroceram* 2014;32(4):283–91.
- [32] Tan X, Xu Z, Shang JK, Han P. Direct observations of electric field-induced domain boundary cracking in (001) oriented piezoelectric $\text{Pb}(\text{Mg}_{1/3}\text{Nb}_{2/3})\text{O}_3$ -PbTiO₃ single crystal. *Appl Phys Lett* 2000;77(10):1529–31.
- [33] Tan X, Shang JK. In-situ transmission electron microscopy study of electric-field-induced grain-boundary cracking in lead zirconate titanate. *Philos Mag A* 2002;82(8):1463–78.
- [34] Tan X, He H, Shang J-K. In situ transmission electron microscopy studies of electric-field-induced phenomena in ferroelectrics. *J Mater Res* 2005;20(7):1641–53.
- [35] Daniels JE, Jo W, Rödel J, Honkimäki V, Jones JL. Electric-field-induced phase-change behavior in $(\text{Bi}_{0.5}\text{Na}_{0.5})\text{TiO}_3$ -BaTiO₃-($\text{K}_{0.5}\text{Na}_{0.5})\text{NbO}_3$: a combinatorial investigation. *Acta Mater* 2010;58(6):2103–11.
- [36] Kutnjak Z, Rožič B, Pirc R. Electrocaloric effect: theory, measurements, and applications. Wiley Encyclopedia of Electrical and Electronics Engineering, John Wiley & Sons, Inc; 2015.
- [37] Scott JE. Electrocaloric materials. *Annu Rev Mater Res* 2011;41(1):229–40.
- [38] Moya S, Defay E, Heine V, Mathur ND. Too cool to work. *Nat Phys* 2015;11(3):202–5.
- [39] Ahn CW, Hong C-H, Choi B-Y, Kim H-P, Han H-S, Hwang Y, Jo W, Wang K, Li J-

- F, Lee J.-S, Kim I.W. A brief review on relaxor ferroelectrics and selected issues in lead-free relaxors. *J Korean Phys Soc* 2016;68(12):1481–94.
- [40] Bokov AA, Ye ZG. Recent progress in relaxor ferroelectrics with perovskite structure. *J Mater Sci* 2006;41(1):31–52.
- [41] Cross LE. Relaxor ferroelectrics, piezoelectricity. Springer Berlin Heidelberg; 2008. p. 131–55.
- [42] Schmidt G, Arndt H, Borchhardt G, von Cieminski J, Petzsche T, Borman K, Sternberg A, Zirnite A, Isupov VA. Induced phase transitions in ferroelectrics with diffuse phase transition. *Phys Status Solidi A* 1981;63(2):501–10.
- [43] Kamba S, Bovtun V, Petzelt J, Rychetsky I, Mizaras R, Brilingas A, Banys J, Grigas J, Kosec M. Dielectric dispersion of the relaxor PLZT ceramics in the frequency range 20 Hz–100 THz. *J Phys: Condens Matter* 2000;12(4):497.
- [44] Qu W, Zhao X, Tan X. In situ transmission electron microscopy study of the nanodomain growth in a Sc-doped lead magnesium niobate ceramic. *Appl Phys Lett* 2006;89(2):022904.
- [45] Qu W, Zhao X, Tan X. Evolution of nanodomains during the electric-field-induced relaxor to normal ferroelectric phase transition in a Sc-doped $\text{Pb}(\text{Mg}_{1/3}\text{Nb}_{2/3})\text{O}_3$ ceramic. *J Appl Phys* 2007;102(8):084101.



Xiaoli Tan is a professor of materials science and engineering at Iowa State University of Science and Technology. He obtained his PhD degree from the University of Illinois at Urbana Champaign in 2002. He received an NSF CAREER Award in 2004. He is an associate editor of the *Journal of the American Ceramic Society*. His research focuses on the structure–property relationship in electroceramics, with *in situ* transmission electron microscopy as the primary characterization tool. He has published more than 130 articles.



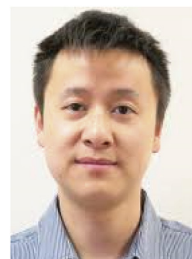
John E. Daniels is an associate professor in the School of Materials Science and Engineering at the University of New South Wales, Australia. He received his BS and PhD degrees in physics in 2003 and 2007, respectively, from Monash University, Australia. He completed postdoctoral research at The European Synchrotron, where he studied instrumentation and measurement methods for materials characterization. His research interests focus on structural measurement by scattering methods and electromechanical materials.



Wook Jo is a professor at the School of Materials Science and Engineering, Ulsan National Institute of Science and Technology (UNIST), South Korea. Prior to joining the faculty of UNIST in 2014, he had served as a group leader for the Processing of Ferroelectrics Lab at the Institute of Materials Science, Technische Universität Darmstadt, Germany, since 2007. His recent research focuses on the functional properties of ferroelectric materials with special emphasis on lead-free piezoceramics and relaxor ferroelectrics. He has published more than 140 papers, seven books, and holds six patents.



Chang-Hyo Hong is a postdoctoral research associate at Prof. Wook Jo's group in Ulsan National Institute of Science and Technology (UNIST), South Korea. He received his Ph.D. from UNIST in 2018. His graduate research focused on the chemically- and electrically-induced phase transitions of relaxor ferroelectrics. His research interests are mainly on fundamental analysis of relaxor ferroelectrics, lead-free piezoceramics, and their applications.



Hanzheng Guo is a senior development engineer at KEMET Electronics Corporation. He obtained his Ph.D. in Materials Science and Engineering from Iowa State University in 2014, focusing on *in situ* TEM study of the microstructural mechanisms for electric-field-induced phenomena in piezoelectrics and ferroelectrics. His current research interests focus on design-processing-structure-property relationships for ceramic-based materials.